

DEPARTMENT OF PHYSICS



NAME: Matthew French
DEGREE: Physics MSci
PROJECT/DISSERTATION NUMBER: PA7
TITLE: Lepton Flavour Violation in Decays of Tau Leptons at CMS
YEAR OF SUBMISSION: 2005
SUPERVISOR: Dr. Helen Heath



H. H. Wills Physics Laboratory
University of Bristol
Tyndall Avenue, Bristol BS8 1TL

Contents

Title	1
Contents	2
Acknowledgements	3
Abstract	4
1 Introduction	5
1.1 Aims	5
1.2 The Standard Model	5
1.3 The Large Hadron Collider (LHC)	5
1.4 CMS	6
1.4.1 Tracker	7
1.4.2 ECAL	7
1.4.3 HCAL	8
1.4.4 Magnet System	9
1.4.5 Muon Chambers	9
1.4.6 CMS Trigger	10
2 Detailed Background	11
2.1 Lepton Flavour Conservation and Violation	11
2.2 Neutrino Mixing	11
2.3 Neutrino Mass & Oscillations	11
2.4 Extensions of the SM	12
2.5 Previous Experimental Searches	13
2.6 Backgrounds	13
2.7 Current Experimental Limits	14
2.7.1	14
2.7.2 Other Relevant Branching Ratios	14
2.8 Cross Section and Number of Events	14
3 Experiment & Results	15
3.1 The $\tau \rightarrow \mu \gamma$ Decay	15
3.1.1 PYTHIA & CMKIN - The Generator Simulator	15
3.1.2 ROOT	15
3.1.3 Initial Investigations	15
3.1.4 Tau Reconstructed Mass	16
3.1.5 Final Cuts	16
3.1.6 Tau Reconstructed Mass Generator Level Graph	17
3.1.7 FAMOS - The Detector Simulator	17
3.1.8 Tau Reconstructed Mass Detector Level Graph	17
3.1.9 Other Detector Level Graphs	18
3.2 The $\tau \rightarrow e \gamma$ Decay	18
4 Analysis	19
4.1 The $\tau \rightarrow \mu \gamma$ Decay	19
4.2 The $\tau \rightarrow e \gamma$ Decay	19
5 Discussion & Conclusion	20
5.1 The $\tau \rightarrow \mu \gamma$ Decay	20
5.2 The $\tau \rightarrow e \gamma$ Decay	20
References	21

$\tau \rightarrow \mu \gamma$
 $\tau \rightarrow e \gamma$

Acknowledgements

I would like to thank my project supervisor, Dr. Helen Heath, for her assistance and suggestions throughout the project, my project partner Liam Malone and David Evans, a fellow project student, for his assistance with some of the computing aspects of the project.

Abstract

This project used the CMKIN and FAMOS software programmes to simulate the generation and detection of the lepton flavour violating processes $\tau \rightarrow \mu \gamma$ and $\tau \rightarrow e \gamma$ at CMS. The major backgrounds were identified as $\tau \rightarrow \mu \nu_\tau \nu_\mu \gamma$ and $\tau \rightarrow e \nu_\tau \nu_e \gamma$ respectively. In contrast with previous investigations the taus investigated were from $Z \rightarrow \tau \tau$ decays. The tau mass reconstructed from only the muon and photon was found to be the best parameter for background-signal differentiation. If no signal is observed in 100 fb^{-1} of data then this project shows the limit CMS can place at 90% CL is $BR(\tau \rightarrow \mu \gamma) \leq 3.63 \times 10^{-7}$. This is consistent with other work focusing on taus from $W \rightarrow \tau \nu_\tau$ decays at CMS and also with limits ATLAS may place. No improvement on current limits was achieved for $\tau \rightarrow e \gamma$.

1 Introduction

1.1 Aims

This project aimed to use both generator and detector level software simulations of the Compact Muon Solenoid (CMS) detector to investigate the lepton flavour violating (LFV) decays $\tau \rightarrow \mu \gamma$ and $\tau \rightarrow e \gamma$. It looked for ways in which the signatures of these decays could be distinguished from their backgrounds and what limits the CMS experiment may put on the branching ratios if no signal is observed.

1.2 The Standard Model

Currently there are believed to be four fundamental forces responsible for all interactions found in nature. The Standard Model (SM) describes three of these forces; the electromagnetic force, the weak force and the strong force. Gravity is not incorporated into the SM since no satisfactory quantum theory of gravity exists. The forces described in the SM correspond to gauge symmetries (i.e. they are invariant under a local rotations), the gauge group of the SM is $SU(3) \times SU(2) \times U(1)$. Where $SU(3)$ describes the non-abelian symmetry of colour charge, $SU(2)$ describes the non-abelian symmetry of weak isospin and $U(1)$ describes the abelian symmetry of weak hypercharge.

The electromagnetic (EM) force acts on all particles or objects carrying electrical charge. It is mediated by massless photons (spin 1) and has an infinite range. The theory describing EM interactions is Quantum Electrodynamics (QED).

The weak force is propagated by 3 massive bosons, W^+, W^-, Z^0 (all spin 1). Due to their large masses ($m_W \approx 80 \text{ GeV}$ and $m_Z \approx 91 \text{ GeV}$) the weak force has a very short range: $O(10^{-18} \text{ m})$. The weak force only acts on left handed particles and right handed anti-particles.

The strong force acts on objects with a net colour charge and is carried by a series of eight massless, self interacting, coloured gluons (all spin 1). The strong force binds quarks together in mesons and baryons, acts over a distance $O(10^{-15} \text{ m})$ and gets stronger at larger distances. The theory describing strong interactions is called Quantum Chromodynamics (QCD).

The final force, gravity, is very weak over short distances in comparison with the other three forces. It has an infinite range and acts on all massive bodies. It has been widely suggested, although not proved, that gravity is mediated by gravitons (spin 2).

The electromagnetic and weak forces have been unified (shown to be two aspects of the same force) giving the electro-weak force. Electro-weak symmetry is spontaneously broken through the existence of the postulated Higgs field leading to the large masses of the W^+, W^-, Z^0 but leaving the photon massless.

The SM also describes twelve matter particles (and their associated anti-particles – a requirement from quantum mechanics): three quark flavour doublets and three flavours of leptons with corresponding neutrinos (electron, muon and tau).

$$\text{quarks} : \begin{pmatrix} u \\ d \end{pmatrix} \begin{pmatrix} c \\ s \end{pmatrix} \begin{pmatrix} t \\ b \end{pmatrix} \quad \text{leptons} : \begin{pmatrix} e \\ \nu_e \end{pmatrix} \begin{pmatrix} \mu \\ \nu_\mu \end{pmatrix} \begin{pmatrix} \tau \\ \nu_\tau \end{pmatrix}$$
$$\text{gauge bosons} : \gamma, Z^0, W^+, W^-, g$$

Fig(1.2.a) – SM Particles

The up, charm and top quarks have electrical charge +2/3 and the down, strange and bottom quarks have electrical charge -1/3. Quarks also have colour charge, whilst not in any way related to the everyday concept of colour (the 'size' of a quark is much smaller than the wavelength of visible light) the charge states are commonly called red, green and blue. Colour charged particles appear to be confined in colour neutral combinations such as mesons (quark and anti-quark), baryons (three quarks) and possibly pentaquarks [1] (four quarks and an anti-quark). There is mixing between the three generations of quarks, which is parametrised by the CKM matrix.

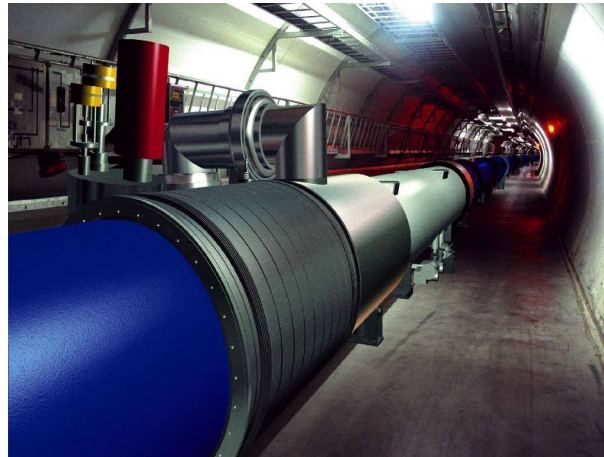
The electron, muon and tau have a charge of -1. Lepton universality indicates muons and taus should have the same properties as electrons except for differences derived from the effects of their larger masses. The three neutrinos carry no charge, and recent evidence suggests they have very small, rather than zero, masses [2]. In its simplest form the SM has around 19 parameters which must be inserted by hand and cannot be predicted – hence it is a model and not a theory.

1.3 The Large Hadron Collider (LHC)

The LHC [3] will be the largest and most powerful particle accelerator ever built when its construction at the CERN laboratory in Geneva, Switzerland is completed in 2007. It will consist of a sixteen mile ring of superconducting dipole magnets in the old LEP tunnel 100m underground, numerous pre-accelerators and four main experiments. It will collide two beams of protons at a centre-of-mass energy of up to 14TeV, initially at a luminosity of $10^{33} \text{ cm}^{-2} \text{ s}^{-1}$ and eventually at $10^{34} \text{ cm}^{-2} \text{ s}^{-1}$ [4] or beams of heavy ions such as lead at energies of up to 1250TeV.

The protons will be injected into the LHC from the Super Proton Synchrotron (SPS) and its pre-accelerators at 0.45TeV and accelerated to 7TeV. Protons grouped together into bunches will rotate in opposite directions around the ring before being collided at one of the experiments. A series of dipole magnets producing a magnetic field of 8.36T along with other magnets for small corrections (approximately 5000 in total) will be required to keep the protons travelling around the ring.

Placed at different sites around the ring will be the experiments themselves: ALICE which is a heavy ion detector, ATLAS and CMS which are both general purpose detectors and LHCb which is designed to detect differences between matter and anti-matter.



Fig(1.3.a) – A computer generated image of the LHC installed in the LEP tunnel [5]

1.4 CMS [6]

CMS is a general purpose detector designed to measure the energy and momentum of photons and charged particles (such as electrons and muons) with very high precision. The detector is designed to cover a pseudorapidity

$|\eta| < 5$ (where $\eta = -\ln(\tan \frac{\theta}{2})$ and θ is shown in Fig(1.4.c)) and primarily consists of a silicon tracker, an

Electromagnetic CALorimeter (ECAL), a Hadron CALorimeter (HCAL), a magnet system and muon chambers.

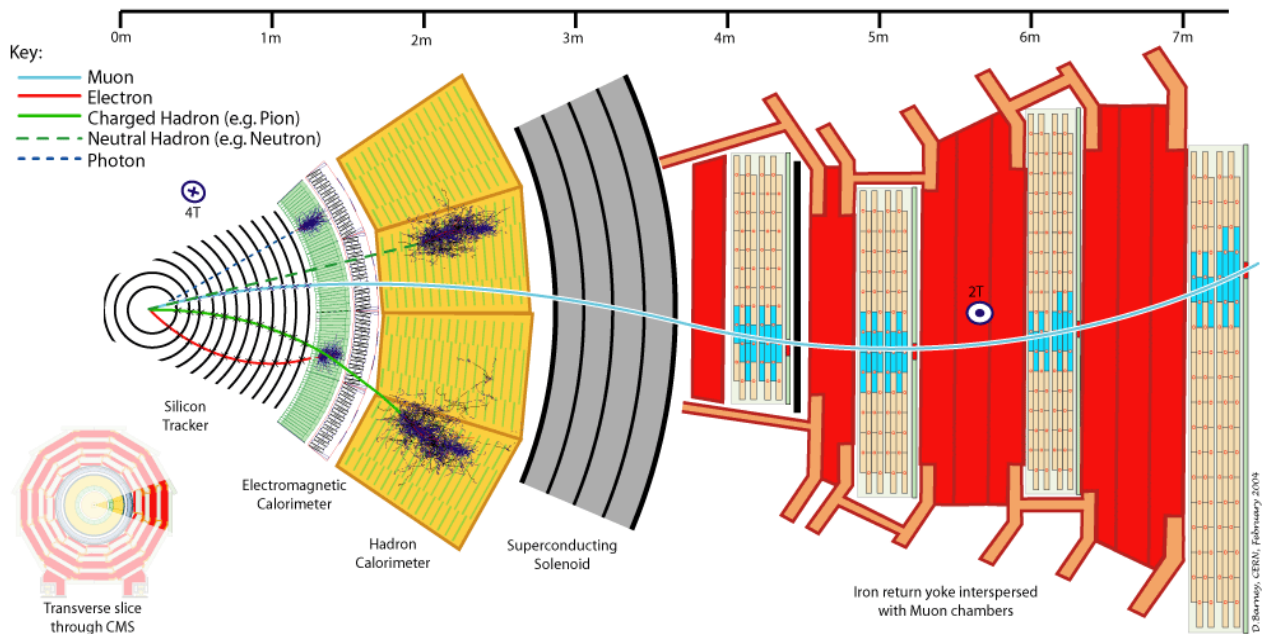
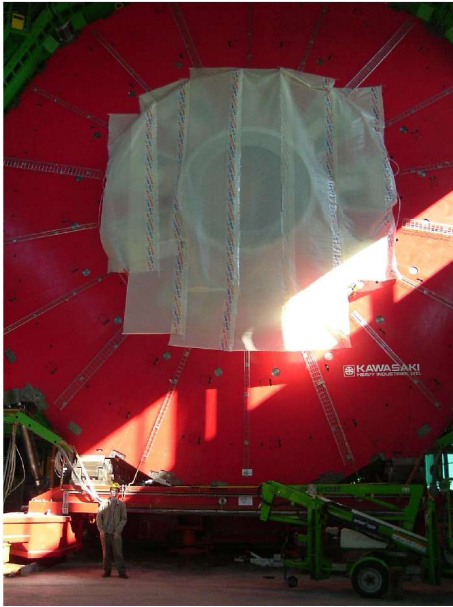
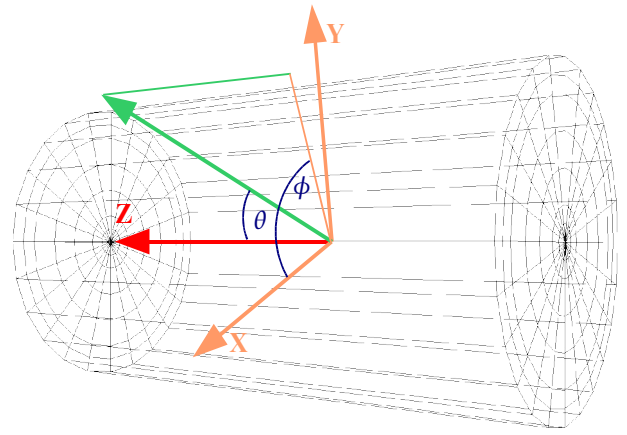


Fig (1.4.a) – Transverse segment of the CMS detector [6]



Fig(1.4.b) – Photo of the CMS detector under construction



Fig(1.4.c) – CMS geometry: beam direction along Z axis, X-Y is transverse plane, $\eta=0$ is in transverse plane, $\eta=5$ is approximately along Z axis

The tracker, ECAL and HCAL are situated inside the solenoid which creates a magnetic field of 4T. The detector will be 21.5m in length, have a diameter of 15m and weigh around 12,500 tonnes.

1.4.1 Tracker

The tracking system is designed to reconstruct high-pT muons, isolated electrons and hadrons with high momentum resolution and high efficiency in the range $|\eta| < 2.5$. It will also be used for accurate production vertex identification and location. To minimise the effects of photon conversions and electron bremsstrahlung the tracking system is designed so that there is a minimum of material in front of the ECAL. To achieve this it is constructed from a combination of silicon strip detectors (in low occupancy regions) and silicon pixel detectors (in high occupancy regions) and provides a set of co-ordinate measurements of sufficient precision and accuracy that track reconstruction can be performed using only a small number of measurements per track. The magnetic field directs low-pT particles into helical paths with a small radius thus reducing the occupancy in the detector at larger radius. The fine granularity of the tracker gives a 95% reconstruction efficiency for charged hadrons with pT above 10GeV; for high energy electrons of 90% and if the tracking system is combined with the muon chambers the efficiency for muons is 98%.

1.4.2 ECAL

The ECAL is designed to measure the energies of electrons and photons with high precision. The barrel section will cover a pseudorapidity of $|\eta| < 1.48$ and the end caps will cover $1.48 < |\eta| < 3.0$, although the highest precision measurement stops at $|\eta| < 2.6$. An additional preshower detector will be installed in the endcap region to provide $\gamma - \pi^0$ separation.

The ECAL consists of 80,000 crystals of lead tungstate (PbWO_4). PbWO_4 was chosen since it has a short radiation length (i.e. a small amount is needed to contain the shower so that the calorimeter is compact), a small Moliere radius, it is a fast scintillator and is relatively easy to produce. The crystals have a cross section of about 22mm x 22mm which matches the Moliere radius of 21.9mm and to limit leakage at the rear end they have a depth of 26 radiation lengths (23cm). PbWO_4 is naturally radiation hard, but optimisation significantly reduces radiation damage. Recent research has concluded that high levels of radiation do not affect the scintillation mechanism or the uniformity of the light yield along the crystal; it only affects the transparency of the crystals but a monitoring system is able to correct for this.

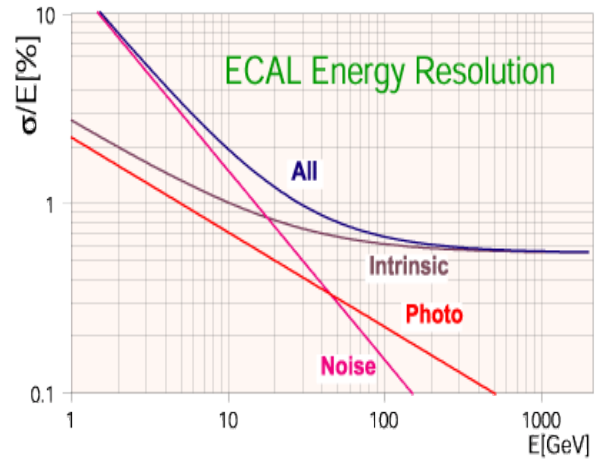
The scintillation light from crystals is captured by either an avalanche photodiode or a vacuum phototriode and converted to a current. Since the light yield is relatively low, there is a pre-amplification stage where the signal is amplified then digitised, and to avoid the design and construction of a large quantity of radiation-hard electronics, the data is transported via a fibre-optic link to be recorded.

Photons do not show up in the tracker but deposit energy in the ECAL, so the signal for a photon is an energy deposit with no track pointing to it.

The energy resolution has been parametrised to include a term arising from photo statistics, a term arising from EM noise and a constant term. This is graphed in Fig(1.4.2.b).



Fig(1.4.2.a) - $PbWO_4$ crystal and avalanche photodiode used in the ECAL



Fig(1.4.2.b) – The different contributions to the ECAL energy resolution

1.4.3 HCAL

The HCAL [7] is designed to measure quark, gluon and neutrino directions & energies by measuring missing transverse energy and the direction & energy of jets. In conjunction with the tracker, ECAL and muon chambers it will also help with the identification of electrons, photons and muons. The immediate transportation of the data away from the ECAL via fibre-optics described above, together with the optimisation of support structures means that the ECAL has a small radius allowing space for additional HCAL layers which improve the overall detector performance.

The hadron barrel (HB) and hadron endcap (HE) calorimeter systems cover the central pseudorapidity range ($|\eta| < 3$). Since the HB and HE feel the 4T magnetic field they are made from alternate layers of 50mm thick copper and stainless-steel (i.e. non-magnetic) absorber plates and 4mm thick scintillator tiles. The readout from the tiles is via wavelength shifting fibres. The HB is approximately 5 interaction lengths thick which is not sufficiently thick to contain all the energy from high energy showers so additional scintillation layers are placed just outside the solenoid providing a combined thickness of around 11 interaction lengths.

For accurate missing energy calculations, the pseudorapidity range covered is extended to $3 < |\eta| < 5$ by the use of forward calorimeters (HF) placed 6m downstream in each direction from the HE. Since the HF will be located in a region of high radiation it uses quartz fibres embedded in steel absorber plates and is mainly sensitive to Cerenkov light from neutral pions.



Fig(1.4.3.a) - The HCAL under construction

1.4.4 Magnet System

The 4T magnetic field created by the superconducting solenoid magnet provides for high momentum resolution by bending the trajectories of electrically charged particles to a degree according to their mass. The magnetic flux generated is returned via an iron yoke. The yoke is a twelve sided cylindrical structure with endcaps and

is divided into layers – some of which can be seen in red in Fig(1.4.5.a).



Fig(1.4.4.a) - Superconducting solenoid magnet

1.4.5 Muon Chambers

The muon chambers are designed to identify and provide a precise measurement of the momentum of muons in association with the tracker. There are four stations (or layers) interleaved with the iron return yoke of the magnet. Muon identification is aided by the large thickness of absorber material (the iron return yoke) which absorbs particles other than muons and neutrinos; there are approximately ten interaction lengths of material before the inner muon station and a further ten before the outer station. Before an energy deposit is identified as a muon a hit must line up in at least two of the four stations. The accuracy of the system is greatly improved by having multiple layers of chambers in each station. It is expected that a resolution of up to $15 \mu m$ will be obtained. A major feature of the muon system is that it allows for the identification of muons and the estimation of their pT in real time for triggering purposes. It also has to be highly efficient in rejecting background hits that look like genuine muons. These backgrounds primarily come from particles which escape through the HCAL, debris from muon interactions with matter, thermal neutrons, beam halo in the forward direction and electronics noise. The muon system as a whole combines information from a variety of different muon detectors – resistive plate chambers (barrel and endcaps), drift tubes (barrel) and cathode strip chambers (endcaps).



Fig(1.4.5.a) – Iron return yoke with spaces for muon chambers



Fig(1.4.5.b) - Muon chambers installed between rings of iron return yoke

1.4.6 CMS Trigger

Approximately 1×10^9 interactions will take place every second but the maximum data transfer rate allows only around 100 of these events to be fully recorded. The trigger system is designed to look at basic information about an event in real time and record only the events in which something interesting occurs. There are a series of triggers for different types of events, the set relevant to this project are {[muon-pT > 25GeV] or [photon-

$p_T > 35 \text{ GeV}$] or $[\text{muon-}p_T > 5 \text{ GeV and photon-}p_T > 15 \text{ GeV}]$. A further cut of $[|\eta| < 2.5]$ is also applied.

2 Detailed Background

2.1 Lepton Flavour Conservation and Violation

The electron neutrino was postulated by Pauli, named by Fermi and was first detected by Reines [8] in 1956 – at the time it was thought to be the only neutrino. However in 1962 Lederman, Schwartz and Steinberger [9] observed charged pions decaying into a muon and a new neutrino which, on combination with a neutron only produced a proton and a negatively charged muon – never a negatively charged electron. This was the foundation for the idea of lepton flavour conservation: the idea that a lepton can only change into another lepton of the same flavour and that a lepton and an antilepton of the same flavour must be created and annihilated together.

Neutrinoless decays of taus and muons are not included in the framework of the SM because they violate charged lepton flavour (and/or baryon) number. The Noether theorem [10] associates a symmetry of the Lagrangian with conservation of a quantity and visa versa. For example if a theory is invariant under rotational transformations then it conserves angular momentum. In the SM the Lagrangian of an interaction field is frequently written to be symmetric under rotations in flavour space. Therefore it could be expected that the interaction will conserve flavour. However, there is no rigorous theoretical justification for lepton flavour conservation and some extensions of the SM predict its violation.

2.2 Neutrino Mixing

The quarks propagate in mass eigenstates which are different mixtures of the flavour eigenstates. Since the mass eigenstates propagate at different speeds the components of a flavour eigenstate get out of phase with each other i.e. a quark starting as one flavour soon looks like another flavour. The same principle can be applied to lepton flavours. Until recently it was thought that neutrinos were massless meaning they would travel at the speed of light and the mass eigenstates would never get out of phase with each other. In fact neutrinos do have a small mass and their mixing is described by the MNS [11] matrix (analogous to the CKM matrix for quark mixing) which relates their interaction eigenstates to their mass eigenstates via three coupling angles $\theta_{12}, \theta_{13}, \theta_{23}$.

2.3 Neutrino Mass & Oscillations

A simple quantum mechanical two neutrino derivation clearly shows that if the probability for neutrino oscillations (NO) is non-zero there is a difference in the masses of the two neutrinos i.e. at least one neutrino has mass. The derivation assumes that there is mixing between the neutrino mass and weak interaction eigenstates.

$$\begin{pmatrix} \nu_\mu \\ \nu_\tau \end{pmatrix} = \begin{pmatrix} \cos\theta & -\sin\theta \\ \sin\theta & \cos\theta \end{pmatrix} \begin{pmatrix} \nu_1 \\ \nu_2 \end{pmatrix} \quad \text{Equation (2.3.a)}$$

$$m_1 \neq m_2 \quad \text{Equation (2.3.b)}$$

Applying the time dependent Schrodinger equation to the mass eigenstates gives:

$$\begin{pmatrix} |\nu_1(r, t)\rangle \\ |\nu_2(r, t)\rangle \end{pmatrix} = e^{ip.r} \begin{pmatrix} e^{-iE_1 t} & 0 \\ 0 & e^{-iE_2 t} \end{pmatrix} \begin{pmatrix} |\nu_1(0)\rangle \\ |\nu_2(0)\rangle \end{pmatrix} \quad \text{Equation (2.3.c)}$$

and using Equation(2.3.a) gives:

$$\begin{pmatrix} |\nu_\mu(r, t)\rangle \\ |\nu_\tau(r, t)\rangle \end{pmatrix} = e^{ip.r} \begin{pmatrix} \cos\theta & -\sin\theta \\ \sin\theta & \cos\theta \end{pmatrix} \begin{pmatrix} e^{-iE_1 t} & 0 \\ 0 & e^{-iE_2 t} \end{pmatrix} \begin{pmatrix} \cos\theta & \sin\theta \\ -\sin\theta & \cos\theta \end{pmatrix} \begin{pmatrix} |\nu_\mu(0)\rangle \\ |\nu_\tau(0)\rangle \end{pmatrix} \quad \text{Equation (2.3.d)}$$

Assuming there is a mu flavour eigenstate at time $t=0$ i.e. $|\nu_\mu(0)\rangle = 1$ and $|\nu_\tau(0)\rangle = 0$, the probability that at a later time, t , there is a tau neutrino instead of the muon neutrino is:

$$P(\nu_\mu \rightarrow \nu_\tau) = |\langle \nu_\tau(r, t) | \nu_\mu(0) \rangle|^2 = \sin^2(2\theta) \sin^2 \frac{(E_1 - E_2)t}{2} \quad \text{Equation (2.3.e)}$$

From previous experiments it is known that the mass of a neutrino is much less than its energy so a few approximations can be made:

$$E_1, E_2 \gg m_1, m_2 \quad \text{and} \quad E_2 - E_1 = \sqrt{m_2^2 + p^2} - \sqrt{m_1^2 + p^2} \approx \frac{m_2^2 - m_1^2}{2p} \quad \text{Equation (2.3.f)}$$

This leads to the final result:

$$P(\nu_\mu \rightarrow \nu_\tau) \approx \sin^2(2\theta) \sin^2 \left(\frac{\Delta m^2 L}{4E} \right) \quad \text{Equation (2.3.g)}$$

This shows neutrino lepton flavour number is not conserved and since there is no requirement in the SM for lepton flavour to be conserved it is possible that charged lepton flavour number may not be conserved.

In reality there are 3 flavours of neutrinos whose mixing is described by a 3×3 matrix with two mass splittings $\Delta_{12} = m_1^2 - m_2^2 = (5.4 - 9.5) \times 10^{-5} eV^2$ and $\Delta_{23} = m_2^2 - m_3^2 = (1.2 - 4.8) \times 10^{-3} eV^2$ and three mixing angles

$0.70 \leq \sin^2(2\theta_{12}) \leq 0.95$, $\sin^2(2\theta_{13}) \leq 0.23$ and $\sin^2(2\theta_{23}) \geq 0.92$ (current values [12] given at the 3σ level).

This would imply that two of the angles θ_{12} and θ_{23} are large and the other θ_{13} is much smaller.

Early indications of NO came from observed deficits in the number of solar electron neutrinos which originate from well understood processes in the sun ($p+p \rightarrow D+e^++\nu_e$ and ${}^8B \rightarrow 2{}^4He+e^++\nu_e$). These were seen by Ray Davis [13] using a chlorine based mechanism ($\nu_e+{}^{37}Cl \rightarrow e^-+{}^{37}Ar$) who reported only 34% of the expected number; the Soviet-American Gallium Experiment (SAGE) [14] and the Italian-German Gallex [15] using Gallium ($\nu_e+{}^{71}Ga \rightarrow e^-+{}^{71}Ge$) who reported 55% of the expected signal and the Japanese Kamiokande light water detector via elastic scattering of neutrinos from electrons who reported 48% of the expected number.

Two pieces of evidence are now recognised as evidence for NO: the atmospheric neutrino deficit and the solar neutrino deficit.

Atmospheric neutrinos result from pion and kaon decays (eg $p+{}^{14}N \rightarrow \pi^++X$, $\pi^+ \rightarrow \mu^+\nu_\mu$, $\mu^+ \rightarrow e^+\nu_e\bar{\nu}_\mu$) in the upper atmosphere. It was expected that the ratio of muon neutrinos to electron neutrinos be about 2, but was observed to be around unity with a characteristic azimuthal angular dependence indicating the presence of neutrino oscillations. The Super Kamiokande collaboration in Japan announced this observation as discovery of neutrino oscillations in 1998 [16]. This has been backed up by results from the Soudan-2 [17] and IMB [18] experiments. These results are consistent with the oscillation of muon neutrinos into tau neutrinos.

Further evidence for the solar neutrino deficit came from the Sudbury Neutrino Observatory in Canada who confirmed NO to 99.999% certainty [19].

Charged electrons, muons and taus don't oscillate since they are mass and flavour eigenstates (if they did oscillate it would be easy to detect due to the dependence of the curvature of particle tracks in a magnetic field on the particle's mass). A possible Feynman diagram for $\tau \rightarrow \mu\gamma$ is shown in Fig(2.3.a) and is based upon neutrino oscillation. However the uncertainty principle indicates that the W can only exist for a very brief period of time ($10^{-26}s$) which is much shorter than the typical period suggested by the above experiments for neutrino oscillation. Thus an extension of the standard model is motivated to explain such a decay, should it occur.

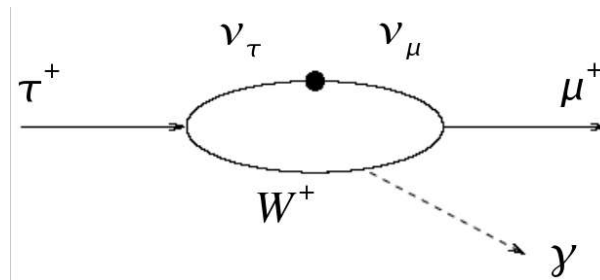


Fig (2.3.a) – Tau decay via neutrino oscillation [20]

2.4 Extensions of the SM

Many extensions of the SM have been proposed which include amongst other things neutrino mass and LFV. None have yet been confirmed, although some have already been ruled out by experimental limits. It is hoped the LHC will point to some physics beyond the SM and which, if any, of the current extensions is the way nature has chosen.

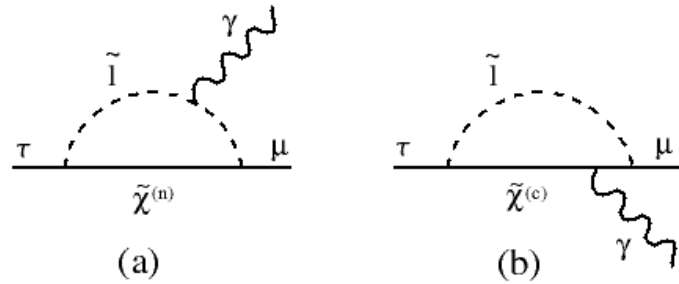
One method neutrino masses can be incorporated into the standard model is by including right-handed neutrinos which can be coupled by Yukawa terms to the left-handed lepton doublet and the Higgs doublet. Neutrino mass terms appear on spontaneous symmetry breaking and allow LFV processes at the one loop level. However the rates for these are proportional $(m_\nu/M_W)^4$ and suppressed by the GIM mechanism giving a branching ratio $O(10^{-50})$ which will be unobservable in the near future. This method also leads to a fine-tuning problem which is explaining why the Yukawa couplings differ by so much.

Partly as a result of this it has been suggested that some supersymmetry (SUSY) based models can accommodate lepton flavour violation [21,22,23]. SUSY postulates boson partners for all SM fermions and fermion partners for all the SM bosons and is frequently based on a SU(5) gauge group.

Another popular method for including neutrino mass is the see-saw mechanism which is used in extensions of the SM such as some SUSY models and the left-right symmetric model – these models contain extra Higgs bosons which lead to Flavour Changing Neutral Currents. LFV branching ratios become $O(m_i^4/m_W^4)$, which could be quite large based upon the current limits for slepton masses. Recent results on the muon anomalous magnetic moment [24], which indicate a difference from the SM value at 2.6σ , also point to the existence of new physics beyond the SM and possibly SUSY.

Further extensions of the SM are Grand Unified Theories (GUT) which include gravity and try to describe all interactions as different aspects of the same fundamental force. Supergravity mediated SUSY is a combination of SUSY and GUT - one minimal SUGRA model [25] predicts $BR(\tau \rightarrow \mu\gamma) \approx 1 \times 10^{-9}$ which could be within reach of experiments in the near future.

Some string theories postulate fermions not included in the SM which mix with the fermions of the SM to produce LFV processes.



Fig(2.4.a) – Generic SUSY Feynman diagrams for $\tau \rightarrow \mu \gamma$. \tilde{l} represents a charged slepton in (a) or sneutrino in (b), $\tilde{\chi}^{(n)}$ represents a neutralino and $\tilde{\chi}^{(c)}$ represents a chargino. [26]

2.5 Previous Experimental Searches

Searches for LFV have taken place at just about every high energy physics laboratory. Searches at LEP's OPAL [27] detector (CERN, Switzerland) have looked for $e^+e^- \rightarrow e\mu, e\tau$ and $\mu\tau$, the L3 [28] and DELPHI [29] detectors also on the LEP experiment have looked for $Z^0 \rightarrow \mu\tau, Z^0 \rightarrow e\tau, Z^0 \rightarrow e\mu$. More recently searches for $\tau \rightarrow \mu \gamma$ have taken place at the BELLE [30] (KEK, Japan) and BaBar [31] (SLAC, USA) detectors. None of these previous searches for lepton flavour violation have claimed a positive discovery nor ruled it out, rather they have set an upper limit on the branching ratio based on non-observation of a signal.

Since the beginning of the LHC project, simulations [32,33] have been performed to lay out a search strategy and to outline what constraint might be put on different branching ratios should a signal not be observed. Due to the very small branching ratio currently placed on $\mu \rightarrow e \gamma$ and $\mu \rightarrow eee$ in comparison with $\tau \rightarrow \mu \gamma$ and $\tau \rightarrow l_{\mu,e} l_{\mu,e} l_{\mu,e}$ these investigations have concentrated mainly upon the decay of a tau produced from the decay of a W. Since the electron is the lightest charged particle, conservation of charge (for which there is a theoretical justification), implies that it doesn't decay.

The results from the L3 and DELPHI experiments detailed above were based on decays of taus produced from electron-positron collisions. These collisions are at a lower energy than will take place at the LHC partly due to synchrotron radiation (the energy given off as synchrotron radiation is inversely proportional to the fourth power of the particle's mass, this is significant for electron-positron colliders, but much less so for the LHC). Obviously an important part of trying to find lepton flavour violation in decays of taus is proving that there was a tau at the beginning. Taus produced from W and Z bosons at the LHC (rather than electron-positron annihilation) can be more energetic so still have a sufficient detection rate despite the higher background. Since investigations have already been performed concentrating on the decays of W bosons, this investigation concentrated on taus produced from the decay of a Z.

2.6 Backgrounds

The most significant background to $\tau \rightarrow \mu \gamma$ is the decay $\tau \rightarrow \mu \nu_\tau \nu_\mu \gamma$ which proceeds via a W^+ . Since neutrinos cannot be detected directly in CMS they will only appear as missing transverse energy. If either the tau, the muon or one of the neutrinos radiate a photon then this could fake the decay $\tau \rightarrow \mu \gamma$. Another background which could contribute is $Z^0 \rightarrow \tau \tau \gamma$ followed by $\tau \rightarrow \mu \nu_\tau \nu_\mu$. Since the branching ratio for this combined decay is significantly smaller than for $\tau \rightarrow \mu \nu_\tau \nu_\mu \gamma$ it was not considered further.

A similar decay, $\tau \rightarrow e \nu_\tau \nu_e \gamma$, is the main background for $\tau \rightarrow e \gamma$.

2.7 Current Experimental Limits

2.7.1 $\tau \rightarrow \mu \gamma$

The current branching ratio published by the particle data group is $BR(\tau \rightarrow \mu \gamma) < 1.1 \times 10^{-6}$ at 90% CL [34].

One of the most stringent current limits is from analysis of $e^+e^- \rightarrow \tau^+\tau^-$ events at a centre-of-mass energy of 10.58 GeV at the BaBar detector at the PEP-II storage ring. They find no evidence for a signal and set an upper limit on the branching ratio of $BR(\tau \rightarrow \mu \gamma) < 6.8 \times 10^{-8}$ at 90% CL [31].

These two branching ratios vary by a factor of approximately 15. Although this may seem a significant amount it can be shown [35] that the value of such an upper-limit approximation can differ by an order of magnitude depending on the precise method involved in the statistical analysis.

2.7.2 Other Relevant Branching Ratios [34]

$$\begin{aligned} BR(\tau \rightarrow \mu \nu_\tau \nu_\mu \gamma) &= 0.0036 \wedge 0.0004 \\ BR(\tau \rightarrow e \gamma) &< 2.7 \times 10^{-6} \text{ at } 90\% \text{ CL} \quad BR(\tau \rightarrow e \nu_\tau \nu_e \gamma) = 0.0175 \wedge 0.0018 \\ BR(\mu \rightarrow e \gamma) &< 1.2 \times 10^{-11} \text{ at } 90\% \text{ CL} \quad BR(\mu \rightarrow e \nu_\mu \nu_e \gamma) = 0.014 \wedge 0.004 \\ BR(Z^0 \rightarrow \tau \tau \gamma) &< 7.3 \times 10^{-4} \text{ at } 95\% \text{ CL} \quad BR(\tau \rightarrow \mu \nu_\tau u_\mu) = 0.1736 \wedge 0.0006 \end{aligned}$$

2.8 Cross Section and Number of Events

Multiplying by the number of seconds in a year (and assuming the experiment will run for approximately one third of the time) and converting to barns, indicates that after one year of running at a luminosity of $10^{33} \text{ cm}^{-2} \text{ s}^{-1}$ the LHC will have generated 10 fb^{-1} of data and after the same period at $10^{34} \text{ cm}^{-2} \text{ s}^{-1}$ there will be 100 fb^{-1} of data.

Assuming 100 fb^{-1} of data and $\sigma(pp \rightarrow Z \rightarrow \tau \tau) = 3 \text{ nb}$ [33], for the BABAR branching ratio there will be upto approximately 20 signal decays and for the higher branching ratio this would increase to 330 both against a background of 1.08 million.

3 Experiment & Results

3.1 The $\tau \rightarrow \mu \gamma$ Decay

3.1.1 PYTHIA & CMKIN - The Generator Simulator

CMKIN/PYTHIA 6.158 [36] was used to simulate the production of a Z^0 and its subsequent decay into a pair of taus: $Z^0 \rightarrow \tau^+ \tau^-$. This was achieved by only allowing Z^0 production (MSTP 1 = 1) and then specifically turning off all other decays of the Z^0 except that to two taus (MDME 174, 1 = 0 ... MDME 189, 1 = 0 except for MDME 186, 1 = 1) [37] and holding decays of taus so as they were real, not virtual (MDCY 15, 1 = 0).

Initially the $\tau \rightarrow \mu \gamma$ kinematics were calculated manually using simple 2 body decay mechanics written in C++ since the decay was not specified in Pythia. The lab axis (different from the lab frame) was defined to have its z axis along the beam direction. In the rest frame of the tau, the tau was 'decayed' into a muon and a photon using conservation of momentum. A random number generator was used to give the angle at which the muon and photon moved off. The momentum components of the muon and photon were resolved parallel and perpendicular to the velocity of the tau rest frame in the lab frame. A relativistic transformation was then applied to the parallel component (no transform is necessary for the perpendicular components). Once these values were in the lab frame they were resolved to the lab axis.

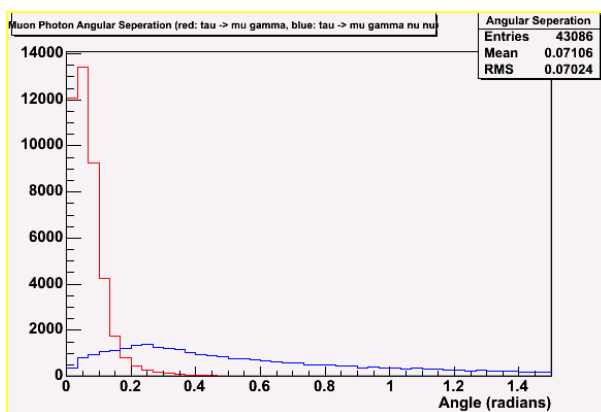
Later, it was discovered that decays could be defined within a Pythia data card. A new sub-process number 4001 (the choice of number is arbitrary provided Pythia hasn't already assigned it) was created. The entry point, i.e. what is supposed to decay via process 4001, is defined by setting MDCY 15, 2 = 4001 where the 15 indicates a tau [38]. MDCY 15, 3 = 1 states that there is only one decay channel and KFDP 4001, 1 = 13 defines that one of the decay products is a muon and KFDP 4001, 2 = 22 that the other is a photon. Other decays not recognised by Pythia (such as the background $\tau \rightarrow \mu \nu_\tau \nu_\mu \gamma$) can be specified in a similar way. In order to speed up the processing time and stay within file size and computational limitations it was decided to limit the number of events in each ntupl to 1000. Therefore in order to analyse, say, 100,000 events, 100 ntupls were generated.

3.1.2 ROOT

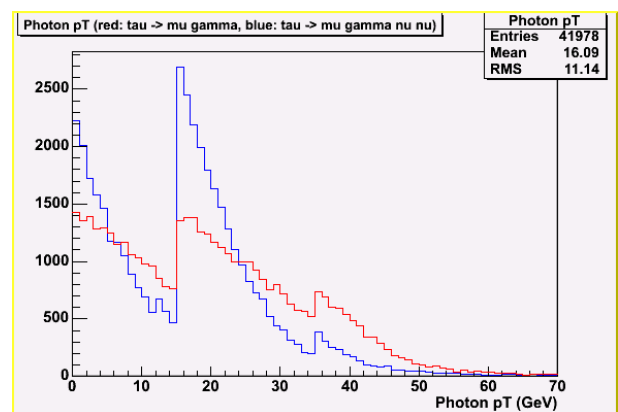
ROOT [39] is an object oriented analysis program that was used to analyse and plot graphs from the data generated. CMKIN created ntupl files in the HEPEVT format which after conversion to root format (using h2root) could be analysed. The HEPEVT format provides various information about the particles involved in each simulated collision: Nhep gives the number of entries in the current collision, Idhep[j] gives the particle ID number according to the Monte Carlo particle numbering scheme [38] of the particle at entry number j and Phep[j][k] gives x momentum (k=0), y momentum (k=1), z momentum (k=2), energy (k=3) and mass (k=4) of the particle at entry number j.

3.1.3 Initial Investigations

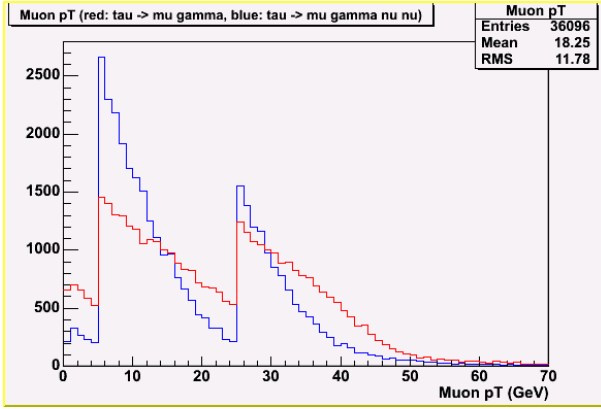
The investigation focused on finding a parameter which would differentiate the signal from the background sufficiently. Since there was a steep learning curve required to use some of the software, initially various parameters were plotted using an equal number of signal and background events. This was still extremely useful since it could always be borne in mind when viewing graphs that the 'real' signal would be significantly smaller. The CMS trigger cuts described in §1.4.6 were applied in the initial analysis.



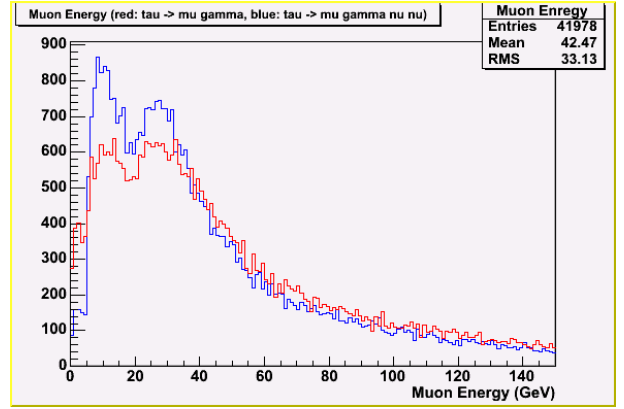
Fig(3.1.3.a) – Muon-photon angular separation with CMS trigger cuts: 1×10^5 background events in blue and 1×10^5 signal events in red



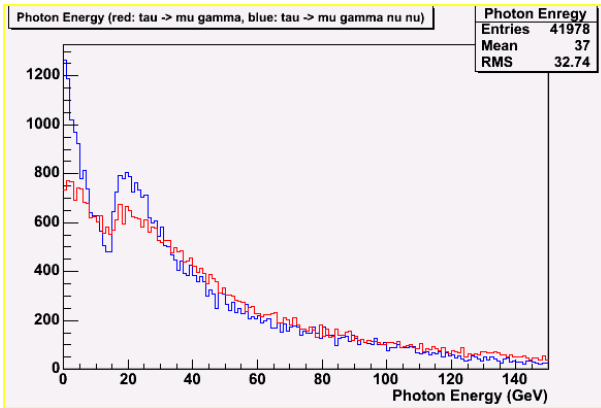
Fig(3.1.3.b) – Photon pT with CMS trigger cuts: 1×10^5 background events in blue and 1×10^5 signal events in red



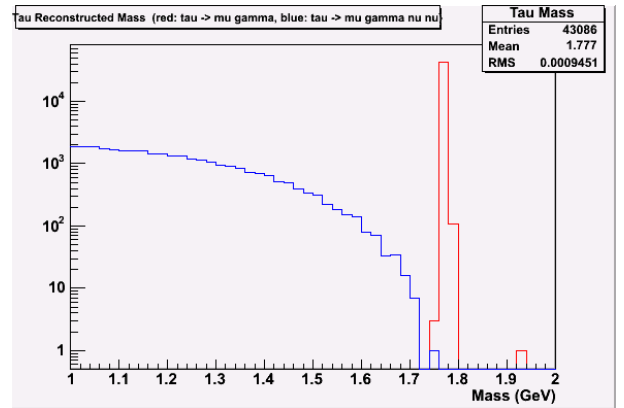
Fig(3.1.3.c) – Muon pT with CMS trigger cuts: 1×10^5 background events in blue and 1×10^5 signal events in red



Fig(3.1.3.d) – Muon Energy with CMS trigger cuts: 1×10^5 background events in blue and 1×10^5 signal events in red



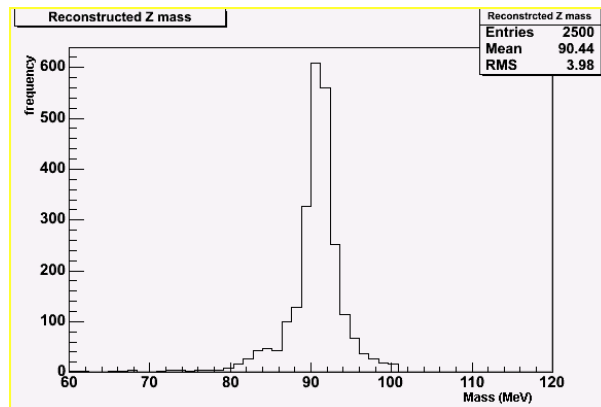
Fig(3.1.3.e) – Photon energy with CMS trigger cuts: 1×10^5 background events in blue and 1×10^5 signal events in red



Fig(3.1.3.f) – Tau reconstructed mass with CMS trigger cuts: 1×10^5 background events in blue and 1×10^5 signal events in red

3.1.4 Tau Reconstructed Mass

The results of the initial analysis – see Figs(3.1.3.a-f) – indicated that the best chance of seeing a signal would come from graphs of the tau reconstructed mass. Where $m_\tau = (E_\mu + E_\gamma)^2 - (p_{\mu x} + p_{\gamma x})^2 - (p_{\mu y} + p_{\gamma y})^2 - (p_{\mu z} + p_{\gamma z})^2$. In order to check that the taus were real i.e. their reconstructed mass was 1.777 GeV, the Z reconstructed mass was plotted.



Fig(3.1.4.a) – The Z reconstructed mass

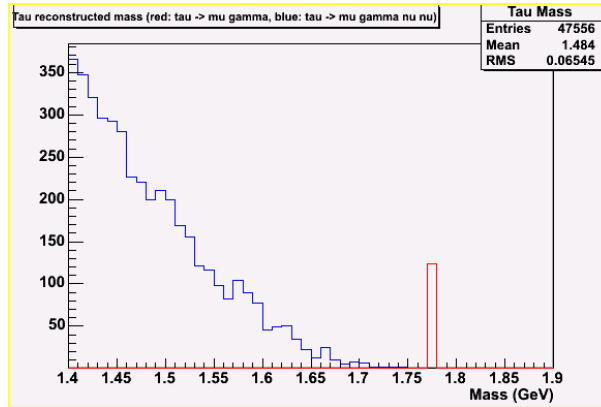
3.1.5 Final Cuts

Since the tau reconstructed mass is 1.777 GeV, background events which would produce an invariant mass of less than 1 GeV were excluded. In conjunction with the CMS trigger cuts detailed in §1.4.6 this allowed a significant proportion of the background to be excluded.

It was realised that a significant reduction in computer processing time could be achieved if a slightly less stringent set of cuts could be applied when the events are generated using Pythia. In order to do this a version of CMKIN was specially compiled [40] to include these cuts. The cuts applied at this stage were $[m_{reconstructed\ \tau} > 1\text{GeV}]$ and $[|\eta| < 2.5]$ and $\{[\text{muon-pT} > 23\text{GeV}] \text{ or } [\text{photon-pT} > 30\text{GeV}] \text{ or } [\text{muon-pT} > 4.5\text{GeV} \text{ and } \text{photon-pT} > 12\text{GeV}]\}$. The output from CMKIN after successfully generating 1000 events which passed these cuts detailed the number of events it had tried. When the total of tries had reached 1.08million, it had actually generated 134,000 which had passed the cuts.

3.1.6 Tau Reconstructed Mass Generator Level Graph

Using the generator level data (i.e. the data from Pythia) a graph was plotted of the tau reconstructed mass for 100fb^{-1} of data. The signal was placed on manually, scaling the 1000 events generated by 0.33 (since 330 events is the number suggested by the branching ratio $BR(\tau \rightarrow \mu \gamma) < 1.1 \times 10^{-6}$).



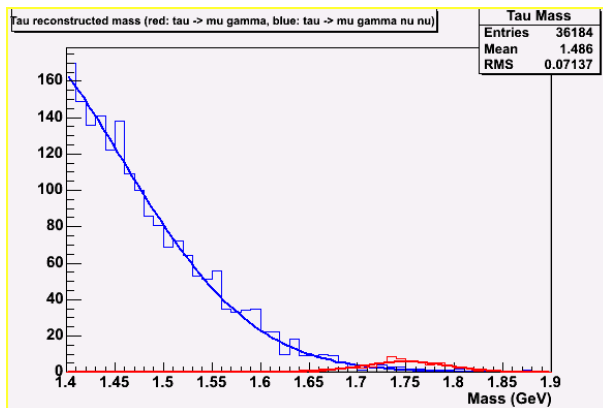
Fig(3.1.6.a) – Generator level tau reconstructed mass with CMS trigger cuts showing background in blue and signal (scaled to $BR(\tau \rightarrow \mu \gamma) < 1.1 \times 10^{-6}$) in red

3.1.7 FAMOS - The Detector Simulator

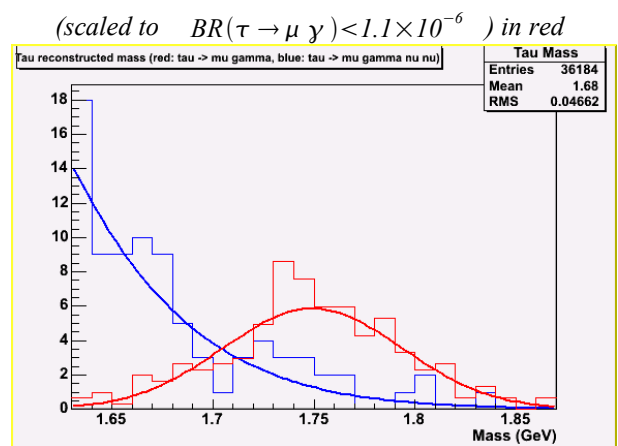
FAMOS (Fast MONte-carlo Simulation) [41] provides a software simulation of CMS based on Monte-Carlo parametrisations of the detector response (FAMOS_1_2_0_pre3 was actual version used). It takes input as ntpl files from the generator simulator and outputs histograms which can be analysed in ROOT. At the expense of some accuracy FAMOS is significantly faster than a GEANT based simulator such as OSCAR/ORCA. Even using FAMOS analysing 134,000 events took nearly 3 days of computer processing time in addition to the 1 day required for the generation stage.

3.1.8 Tau Reconstructed Mass Detector Level Graph

This graph was plotted using the output from FAMOS of the 134,000 background events processed and scaling the 1000 signal events processed by 0.33. The ROOT Fit function was used to fit a Gaussian approximation to the background (G1) and the signal (G2). The parameters of the fit were; G1 : height at mean = 195.409, mean = 1.31996 and standard deviation = 0.135615 & G2: height at mean = 5.86774, mean = 1.74928 and standard deviation = 0.0443782.



Fig(3.1.8.a) - Detector level tau reconstructed mass with CMS trigger cuts showing background in blue and signal

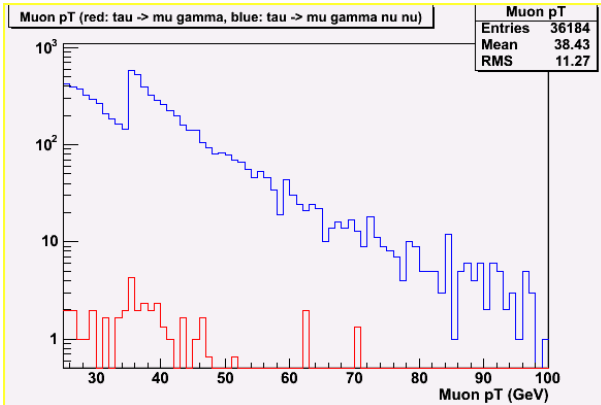


Fig(3.1.8.b) - Detector level tau reconstructed mass with (scaled to $BR(\tau \rightarrow \mu \gamma) < 1.1 \times 10^{-6}$) in red

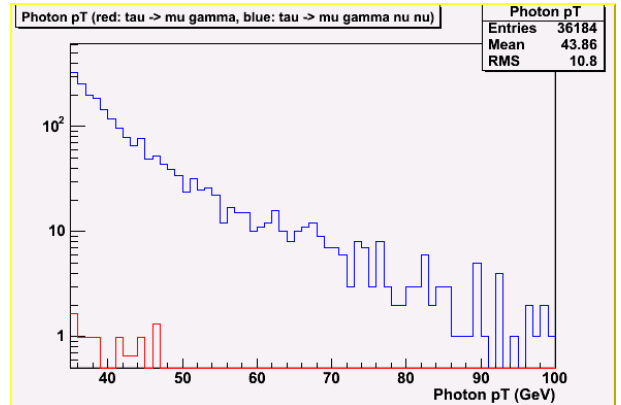
CMS trigger cuts showing background in blue and signal (scaled to $BR(\tau \rightarrow \mu \gamma) < 1.1 \times 10^{-6}$) in red

3.1.9 Other Detector Level Graphs

Fig(3.1.9.a) and Fig(3.1.9.b) back up the earlier assertion that the signal and background can't be distinguished via pT graphs.



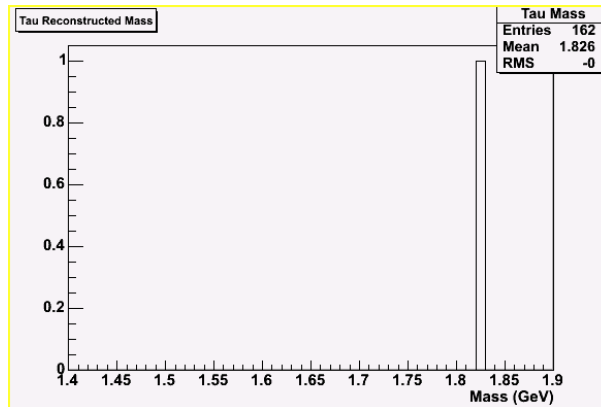
Fig(3.1.9.a) - Detector level muon pT with CMS trigger cuts showing background in blue and signal (scaled to $BR(\tau \rightarrow \mu \gamma) < 1.1 \times 10^{-6}$) in red



Fig(3.1.9.b) - Detector level photon pT with CMS trigger cuts showing background in blue and signal (scaled to $BR(\tau \rightarrow \mu \gamma) < 1.1 \times 10^{-6}$) in red

3.2 The $\tau \rightarrow e \gamma$ Decay

This decay was simulated in exactly the same way as $\tau \rightarrow \mu \gamma$. The output from the detector simulator of signal events (no background events were included) is shown in Fig(3.2.a). From 1000 signal events put through, only one has come out.



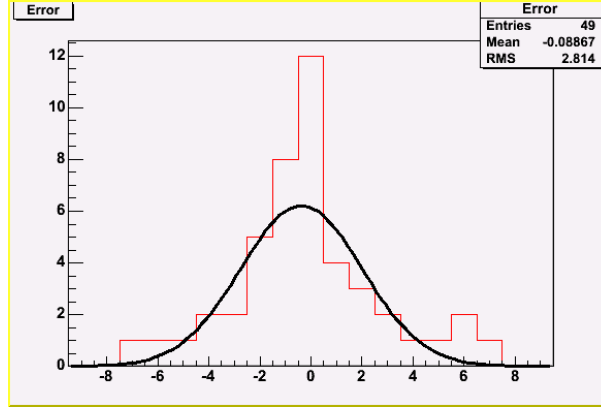
Fig(3.2.a) – Detector level tau reconstructed mass from 1000 events

4 Analysis

4.1 The $\tau \rightarrow \mu \gamma$ Decay

In order to answer the question: “what limit can be placed on the branching ratio should no signal be seen?” the region of tau reconstructed mass between 1.7 and 1.8 was examined.

Looking at the background, it was assumed for each bin that the difference between the number of entries predicted by G1 and the actual number of entries observed was distributed according to a Gaussian (G3) - this is known as the central limit theorem. Two data points (at -20 and -12) were disregarded in order to plot Fig(4.1.a) since these are clearly significantly more than the numbers in the bins between 1.7 and 1.8.



Fig(4.1.a) – Difference between the number of entries predicted by Gaussian (G1) and the actual number observed, with Gaussian (G3) fitted to this distribution

The parameters for G3 were: height at mean = 6.22005, mean = -0.374945 and standard deviation = 2.37980.

For bins in the range 1.7 to 1.8 in Fig(3.1.8.b) the height of G1 was taken as the 'mean' and the standard deviation was taken as that of G3. The height of the fluctuations in the background was calculated at the 90% level. It was then assumed that in order to detect a signal at the 90% level, the signal would need to exceed the height of these fluctuations. For the two central bins, the number of signal events needed for observation was summed providing a total number of signal events required – calculated to be 6.1. The probability of the signal lying between 1.74 and 1.76 accounted for 17.826% of the total signal area so 35 events would actually be needed.

The detection efficiency was then calculated: considering the signal only, since this is in the correct region 314 out of 330 events were picked up by FAMOS giving an efficiency of 95% and so requiring 36 events. From these 314, 104 pass the CMS trigger cuts indicating a total of 109 signal events required.

The number of tau decays in 100 fb^{-1} of data is 3×10^8 , so the branching ratio for 109 events in 3×10^8 is 3.63×10^{-7} . A simple error analysis gives the error on this result as $\pm 0.24 \times 10^{-7}$.

4.2 The $\tau \rightarrow e \gamma$ Decay

Using the same analysis method as for $\tau \rightarrow \mu \gamma$, the fact that only one event was picked up by FAMOS, coupled with the larger background branching ratio leads to a very large $\tau \rightarrow e \gamma$ branching ratio. Even if the background did not overlap the signal and the detector efficiency is not taken into account, the results mean that 1000 events would be required which would lead to a branching ratio of at least 3.3×10^{-6} which is larger than the current limit.

5 Discussion & Conclusion

5.1 The $\tau \rightarrow \mu \gamma$ Decay

The preliminary work done on this decay showed that the only parameter which could distinguish between the signal and background was the tau reconstructed mass. Analysing 100 fb^{-1} gives a result which is consistent (i.e. within an order of magnitude) with the limit of 3×10^{-7} at 90% CL calculated for 100 fb^{-1} of $\tau \rightarrow \mu \gamma$ but with taus from $W \rightarrow \tau \nu$ [33] and a study of the same process for the ATLAS detector simulating 30 fb^{-1} giving a limit of 6×10^{-7} at 90% CL [42].

Fig(3.1.8.b) shows that the mean of the signal distribution is at 1.74928 not the tau mass at 1.777GeV. This is probably due to difference between the Monte-Carlo approximations used in FAMOS and reality, but this is unlikely to affect the overall result since both the background and signal were generated and analysed using the same software and will both be in error by the same amount. The analysis method used does not rely upon the numerical value of the reconstructed mass, only the distribution.

To obtain the average difference between G1 and the actual background data, the region from 1.4 to 1.9 was used rather than the more appropriate region from 1.7 to 1.8 since the smaller region did not provide enough points to which a Gaussian could accurately be fitted. In Fig(4.1.a), two data points at approximately -21 and -12 were neglected. This allowed G3 to be accurately fitted to the remaining data. These two points are far from the 1.7 to 1.8 region and represent a variation vastly greater than the number actually in the bins between 1.7 and 1.8.

Even if different regions are chosen or there are other small differences in the analysis technique used, the final result remains approximately the same to within an order of magnitude as suggested in §2.7.1.

The method of introducing some cuts when the events are generated was very useful since it greatly reduced the processing time required. If this method had not been used around 25 days of processing time would have been needed for 100 fb^{-1} and 75 days for 300 fb^{-1} with FAMOS and more time again for a full detector analysis.

This limit can probably be improved upon by using further cuts to reduce the remaining background. A cut could be placed upon angular separation of the muon and photon (see Fig(3.1.3.a)) and further cuts could be investigated. It would also be valuable to look at larger data samples such as 300 fb^{-1} which should reduce fluctuations between the background & a fitted Gaussian and also the proportion of signal events needed. A full simulation using OSCAR/ORCA would also be valuable despite the computer processing time it would take.

5.2 The $\tau \rightarrow e \gamma$ Decay

FAMOS picked up 162 events out of 1000, of which only one event passed the trigger cuts. For the electrons and photons to be detected by the ECAL there needs to be sufficient separation between them in the detector. More complex analysis, not known to be possible using current versions of FAMOS may make more accurate investigations possible in the future. It was clear that no improvement on the current branching ratio limit could be achieved even if there was no background in the signal region so this decay was not analysed further.

References

- [1] Dzierba A. R., 2004, arXiv.org/hep-ex/0412077
- [2] KamLAND Collaboration, 2004, arXiv.org/hep-ex/0406035
- [3] LHC Website: <http://lhc-new-homepage.web.cern.ch/lhc-new-homepage/>
- [4] CMS ECAL TDR
- [5] Source: <http://intranet.cern.ch/Press/PhotoDatabase>
- [6] CMS Website: <http://cmsdoc.cern.ch>
- [7] CMS HCAL TDR
- [8] Reines F. *et al*, 1956, *Science* **124**, 103
- [9] Lederman L. M., Schwartz M., Steinberger J. *et al*, 1962, *Phys. Rev. Lett.* **9**, 36
- [10] Noether E., 1918, *Nachr. v. d. Ges. d. Wiss. zu Gottingen*, 235 (English translation: Tavel, M. A., 1971, *Transport Theory and Statistical Mechanics* 1(3), 183)
- [11] Maki Z., Nakagawa M., Sakata S., 1962, *Prog. Theo. Phys.* **28**, 870
- [12] Mohapatra R. N., 2004, arXiv.org/hep-ph/0402035
- [13] Davis R. Jr, Harmer D. S. and Hoffman K. C., 198, *Phys. Rev. Lett.* **20**, 1205
- [14] Abasov A. I. *Et al*, 1992, *Phys. Lett. Rev.* **67**, 3332
- [15] Anselmann P. *et al*, 1992, *Phys. Lett. B* **285**, 376
- [16] Fukuda Y. *et al*, 1998, *Phys. Rev. Lett.* **81**, 1562
- [17] Allison W. W. *et al*, 1997, *Phys. Rev. Lett B* **391**, 491
- [18] Casper D. *et al*, 1991, *Phys. Rev. Lett.* **66**, 2561; Becker-Szendy R. *et al*, 1992, *Phys. Rev. D* **46**, 3720
- [19] Ahmad Q. R. *et al*, 2002, *Phy. Rev. Lett.* **89**, 011301 and 011302
- [20] Adapted from: Waltham C., 2003, arXiv.org/physics/0303116
- [21] Ellis J. *et al*, 2000, *Eur. Phys. J. C* **14**, 319
- [22] Feng J. L. *et al*, 2000, *Phys. Rev. D* **61**, 113005
- [23] Hisano J. *et al*, 1996, *Phys. Rev. D* **53**, 2442
- [24] Bennett G.W. *et al*, 2004, *Phys. Rev. Lett.* **92**, 161802
- [25] Hinchliffe I., Paige F. E., 2001, *Phys. Rev. D* **63**, 115006
- [26] Adapted from: Ellis J. *et al*, 2000, *Eur. Phys. J. C* **14**, 319
- [27] OPAL Collaboration, 2001, *Phys. Lett. B* **519**, 23
- [28] L3 Collaboration, 1993, *Phys. Lett. B* **316**, 427
- [29] DELPHI Collaboration, 1993, *Phys. Lett. B* **298**, 247
- [30] BELLE Collaboration, 2004, *Phys. Rev. Lett.* **92**, 171802
- [31] Cottingham N., Private Communication
- [32] Santinelli R., 2003, *Nucl. Phys. B* **123**, 234
- [33] Mazumdar K., 2004, CMS Conference Report: Lepton Flavour Violation at the LHC, CMS CR 2004/013
- [34] Eidelman S. *et al* (Particle Data Group), 2004, *Phys. Lett. B* **592**, 1
- [35] Narsky I., 2000, *Nucl. Instr. And Meth. A* **450**, 444
- [36] Pythia Website: <http://www.thep.lu.se/~torbjorn/Pythia.html>
- [37] http://www.physik.uni-muenchen.de/~schiefer/pythia6.203_decays.html
- [38] Monte Carlo Particle Number Scheme, 1988, *Phys. Lett. B* **204**, 113
- [39] ROOT Website: <http://root.cern.ch>
- [40] Thanks to Dr. Helen Heath for providing a compiled version of CMKIN with cuts
- [41] FAMOS Website: <http://cmsdoc.cern.ch/famos>
- [42] Serin L. and Stroynowski R., 1997, Study of lepton number violating decay $\tau \rightarrow \mu \gamma$ in ATLAS, Report No. ATL-PHYS-97-114